Chemical Engineering Journal 512 (2025) 162661

Contents lists available at ScienceDirect

Chemical Engineering Journal

journal homepage: www.elsevier.com/locate/cej

Intensified and selective recovery of critical metals from aqueous extracts: Fundamentals and system design

Yinghao Wen, Emily L. Tribby, Yuanzhi Tang *

School of Earth and Atmospheric Sciences, Georgia Institute of Technology, 311 Ferst Drive, Atlanta, GA 30332, United States

ARTICLE INFO

Keywords:
Rare earth elements
Critical mineral
Eutectic freeze crystallization
Thermodynamic modeling
Metal–ligand complexation

ABSTRACT

The global transition into a zero-carbon economy is spurring our demand for critical minerals such as rare earth elements (REE), yet the underlying supply chain is unable to keep up the pace. While recovering REE from wastes is a promising solution, improving metal recovery efficiency and the overall economic interest is necessary for technology development. This study developed a system to effectively concentrate and recover REE and multiple valuable metals from the aqueous leachate of a representative waste feedstock (municipal solid waste incineration ash). This modular system consists of four steps. Eutectic freeze crystallization was used as an energy-efficient pre-treatment step to concentrate extracted metals by a factor of ~7–8, reduce reaction volume by over 90%, while remarkably enhancing the efficiency of subsequent metal recovery efficiency. Sulfide precipitation, alkaline precipitation, and oxalate precipitation were then performed to sequentially recover 96.0% Cu and 94.5% Zn, 98.9% Al and 97.0% Fe, and 98.9% REE, respectively, with >98% product purity for each step. Thermodynamic modeling elucidated the important roles of citrate and resulting metal-citrate complexes in protecting target metals from prematurely precipitating out. Carefully designed step-wise addition of precipitating agents outcompetes citrate to form insoluble metal precipitates, enabling sequential and selective metal recovery with high efficiency. Our results highlighted the dual role of citrate as a leaching and protecting agent in metal recovery and the importance of pre-concentration step in enhancing the overall system efficiency. This system can be applied to the intensified resource extraction of other feedstocks as well.

1. Introduction

Rare earth elements (REE) are the "essential vitamins" that fuel our transition from fossil-based energy to a clean energy infrastructure powered by electricity, wind, and solar energy [1,2]. While global energy transition is driving the surging demand for REE, there is a strong consensus that supply chain will soon become the major bottleneck, posing unprecedented pressures to resource exploration, extraction, and manufacturing [2,3]. Because of this, REE have been labeled by the U.S. and European Union as "critical minerals" with high and imminent risk of supply disruption [4]. For decades, REE production predominantly relies on conventional mining of natural deposits, which typically involves energy- and pollution-intensive metallurgical techniques [1,2,5]. Following extraction, hundreds of steps of liquid–liquid extraction using hazardous organic solvents (e.g., kerosene) are repeated to produce purified REE products [6,7]. The estimated cradle-to-gate life cycle impacts of producing 1 kg of REE oxide include: carbon footprint of 105–236 kg CO_2 eq., acidification of 1.14–1.64 mol H^+ eq., ecotoxicity of 525–2020 kg 2,4-D eq., and smog of 14.8–18.9 kg NOx eq [8]. The heavy pollution and high remediation costs associated with traditional mining warrant the search for more sustainable alternative resources and technologies for REE production [9].

Recycling and recovery of REE from secondary or waste feedstocks have great potential to strengthen the REE supply chain, close the material flow loop, reduce environmental pollution, and valorizes wastes [10–13]. REE recovery from different waste feedstocks, including electronic wastes, phosphors, mine tailings, and incineration byproducts, has been under the spotlight of recent research [12,14–23]. However, low REE concentration (total REE of <500 mg/kg) and the co-presence of many interfering metals (e.g., Mg, Al, Ca, Fe) in these wastes raise technical and economic challenges for REE recycling in real applications [13,14,24–27]. In practice, less than 1% of used REE in the U.S. is recycled, most of which come from spent magnets in wind turbines with a relatively high REE content and purity [24]. The recovered REE products in most previous studies typically have low REE and/or high impurity contents, and the other co-extracted metals are not recovered.

* Corresponding author.
E-mail address: yuanzhi.tang@eas.gatech.edu (Y. Tang).

https://doi.org/10.1016/j.cej.2025.162661
Received 26 December 2024; Received in revised form 4 April 2025; Accepted 14 April 2025
Available online 15 April 2025
1385-8947/© 2025 Elsevier B.V. All rights are reserved, including those for text and data mining, AI training, and similar technologies.

In order to maximize the overall economic benefits, technology development for enhanced recovery of REE and other valuable metals is highly desired. After metal extraction, pre-concentration and volume reduction of leachate are also necessary for downstream processing [24]. Eutectic freeze crystallization (EFC) is a novel technique that separates aqueous solutions into pure ice and crystallized solutes by freezing at the eutectic point [28]. It is a more energy-efficient method for water desalination and brine concentration compared to evaporative crystallization and membrane filtration (e.g., enthalpy of fusion for water is only 1/7 of its enthalpy of vaporization) [29].

Strong mineral acids (e.g., HCl and H_2SO_4) have been widely used for REE extraction, which unfortunately comes with heavy chemical input and adverse environmental impacts [30–32]. To overcome these limitations, organic ligands with strong metal complexing ability have been considered as greener alternatives, which can facilitate metal extraction by forming soluble metal–ligand complexes [33–35]. For example, citrate is a biodegradable organic ligand that can effectively extract REE from various feedstocks [36,37]. However, the impacts of leaching ligands on downstream processing and overall metal recovery have been largely overlooked because the ligands of traditionally used mineral acids (e.g., Cl^-) typically have weak complexing ability for metals [34]. For metal recovery processes that involve organic acids, this is especially important because the efficiency and selectivity of post-leaching separation and precipitation processes are largely governed by competitive metal–ligand interactions [38]. Ideally, the selected organic ligand should promote metal leaching from feedstocks by forming soluble metal–ligand complexes. During precipitation, precipitating ligands are added to outcompete the leaching ligand and form insoluble complexes with target metals. Therefore, we aimed to identify a suitable set of leaching/precipitating ligands that can protect target metals from precipitating in premature steps and allow rapid precipitation at the designated step, making sequential and selective metal recovery possible. Developing such a method requires a comprehensive understanding of competitive metal–ligand complexation, and a systematic study in this direction supported by thermodynamic calculation is still missing.

To address these challenges, this study aimed to (1) employ EFC as an energy-efficient physical freezing technique to pre-concentrate metals in the leachate and reduce the leachate volume, (2) develop an effective treatment method for sequential recovery of REE and other valuable metals via three chemical precipitation processes, and (3) elucidate the underlying metal–ligand interactions and impact of citrate on these precipitation processes using thermodynamic modeling. Building upon the characterization of REE and other metal speciation in waste feedstocks such as coal fly ash [25,39–42] and municipal solid waste incineration ash (MSWIA) [43], our recent work demonstrated the high efficiency of citrate-assisted extraction of REE and other metals from MSWIA [12], coal fly ash [14], and REE-bearing carbonate/phosphate minerals [44]. This study uses the citrate leachate from MSWIA as a representative feedstock, and we aimed to maximize the recovery of REE and four other abundant valuable metals (Al, Fe, Cu, Zn). Achieving these objectives will allow us to demonstrate a feasible REE recovery method that integrates physical concentration and chemical precipitation. This intensified recovery method features the selective recovery of REE and multiple valuable metals, which can potentially address the major limitation of existing REE recovery techniques. In addition, elucidating the metal–ligand complexation and dominant metal species involved in each process can provide mechanistic insights for the advantages of using organic ligands compared to mineral acids in metal recovery.

2. Materials and methods

All chemicals used in this study are ACS grade or higher without further purification. MSWIA sample was obtained from a Waste-to-Energy facility located in Northwest USA. Details on the chemicals, MSWIA sample processing, characterization techniques, and analytical methods are discussed in **Supporting Information Text S1–S5**.

2.1. Metal extraction from raw MSWIA sample via citrate leaching

Metals were leached from raw MSWIA using citrate following the same procedures described in our previous work [12]. The metal leaching efficiency was calculated using **Eq. (1)**.

$$Leaching\ Efficiency(\%) = \frac{C_{Leachate} \bullet V_{Leachate}}{C_{Ash} \bullet m_{Ash}} \times 100\% \quad (1)$$

where C_{Ash} and $C_{Leachate}$ (mg/kg) are the metal concentrations in raw MSWIA sample and citrate leachate, respectively; $V_{Leachate}$ (mL) is the leachate volume; m_{Ash} (g) is the mass of MSWIA.

The normalized leaching rates of target metals from raw MSWIA were calculated following the method in our previous work and using the average Brunauer-Emmett-Teller (BET) surface area of MSWIA reported in literatures [35,45].

2.2. Pre-concentration via eutectic freeze crystallization (EFC)

EFC was first performed on a simulated solution containing 10 mmol/L $CaCl_2$ and 10 μmol/L YCl_3 in a fridge (freezing temperature: -20 °C). Every 30 min, samples were collected to measure metal concentrations, and the solution pH, temperature, and volume of solid phase were determined. Based on preliminary results, EFC was then performed on the leachate at a freezing temperature of -20 °C and an optimal reaction time of 450 min. The filtrate (noted as EFC concentrate) was collected via vacuum filtration, and metal concentrations were determined using ICP-MS. The fraction of metals retained in the aqueous phase after EFC is calculated via **Eq. (2)**. The concentration factor is calculated via **Eq. (3)**.

$$Fraction\ retained(\%) = \frac{C_{EFC} \bullet V_{EFC}}{C_{Leachate} \bullet V_{Leachate}} \times 100\% \quad (2)$$

$$Concentration\ Factor = \frac{C_{EFC}}{C_{Leachate}} \quad (3)$$

where C_{EFC} (mg/kg) is the metal concentrations in EFC concentrate; V_{EFC} (L) is the volume of EFC concentrate.

2.3. Sequential metal separation via chemical precipitation

In order to selectively precipitate target metals, three chemical precipitation processes were sequentially performed as described below: Cu and Zn via sulfide precipitation, Al and Fe via alkaline precipitation, and REE via oxalate precipitation. A schematic overview of the overall system is presented in Scheme 1. Dosages of sulfide and oxalate were pre-determined based on the total amount of target metals in feedstocks and reaction stoichiometry. To examine the effect of EFC pre-concentration, the same mass of sulfide and oxalate was added to the EFC concentrate and original leachate without EFC.

(1) Sulfide precipitation for Cu and Zn recovery. 15 mg of sodium sulfide was added to the solutions under stirring and reacted for 30 min. The mixture was filtered via vacuum filtration (pore size 0.2 μm), and the filtrate was collected (noted as sulfide filtrate). The solid product (noted as sulfide product) was dried in an oven at 60 °C overnight and then characterized using X-ray diffraction (XRD) and scanning electron microscopy energy dispersive spectroscopy (SEM-EDX).
(2) Alkaline precipitation for Al and Fe recovery. The solution pH of sulfide filtrate was titrated to 9.0 ± 0.1 using 5.0 mol/L NaOH solution, and the mixture was stirred for 60 min. The increase in solution volume (<1%) was considered when calculating metal concentrations. The solid product (noted as alkaline product) and

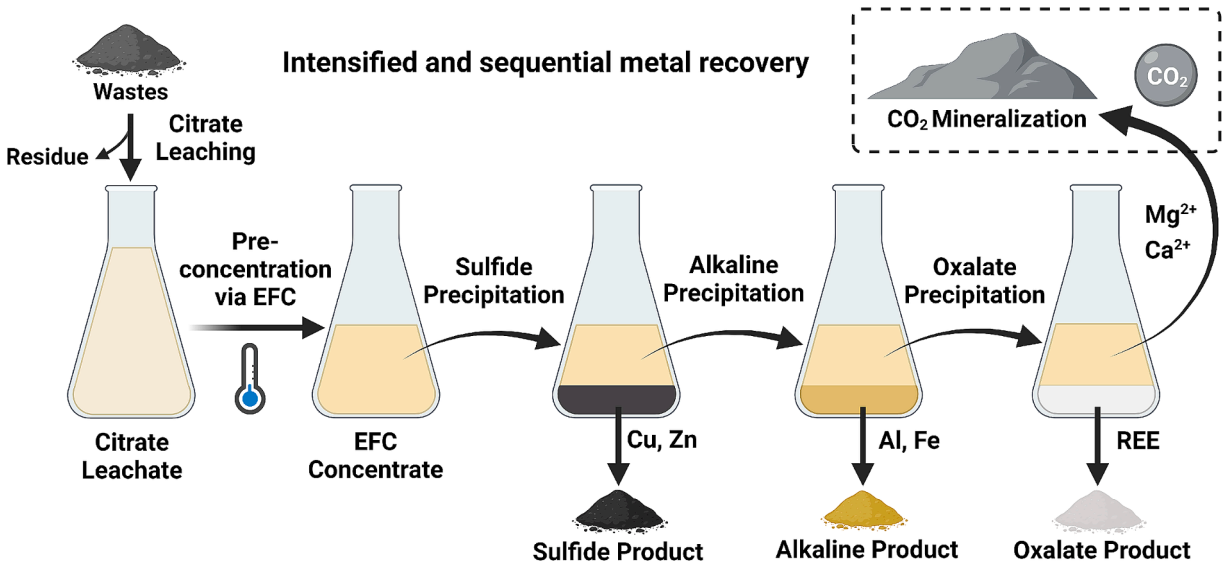

Scheme 1. Schematic overview of intensified and sequential metal recovery process in this study (CO_2 mineralization highlighted in dashed lines is not included in this study).

filtrate (noted as alkaline filtrate) were collected and characterized following the same procedures.

(3) Oxalate precipitation for REE recovery. 10 mg of sodium oxalate was added to the alkaline filtrate under stirring and reacted for 20 min. The solid product (noted as oxalate product) and filtrate (noted as oxalate filtrate) were collected and characterized following the same procedures.

The precipitation efficiency of target metals during each step, their concentrations (mg/kg) in the solid products, enrichment factors compared to raw MSWIA, and overall recovery rate were calculated using **Eqs.** (4)–(7).

$$Precipitation\ Efficiency(\%) = \frac{C_{Pre-reaction} - C_{Filtrate}}{C_{Pre-reaction}} \times 100\% \quad (4)$$

$$Metal\ concentration = \frac{(C_{Pre-reaction} - C_{Filtrate}) \bullet V_{Filtrate}}{m_{Product}} \quad (5)$$

$$Enrichment\ Factor = \frac{C_{product}}{C_{Ash}} \quad (6)$$

$$Overall\ Recovery\ Rate(\%) = \frac{C_{product} \bullet m_{product}}{C_{Ash} \bullet m_{Ash}} \times 100\% \quad (7)$$

where $C_{Pre\text{-}reaction}$ and $C_{Filtrate}$ (mg/kg) are the metal concentrations in the solution before and after precipitation, respectively; $V_{Filtrate}$ (L) is the volume of filtrate; $m_{Product}$ (mg) is the dry mass of solid product; $C_{product}$ (mg/kg) is the metal concentration in solid product calculated by **Eq.** (5).

2.4. Thermodynamic modeling

The thermodynamics of interactions between target metals and different ligands, including major species of metal–ligand complexations and corresponding saturation index (SI) in each precipitation process were calculated using the software PHREEQC version 3. Input of solution chemistry was based on experimental measurements and was summarized in Table S1. The *minteq.v4.dat* database with additional stability constants (logβ) of metal–ligand complexes introduced from the NIST Standard Reference Database (SRD) 46 (critically selected stability constants of metal complexes) and literatures was used for modeling [34,46–61]. Values of logβ reported at ionic strength (I) > 0 were corrected to $\log\beta^0$ (at $I = 0$) as described in **Text S6**. The calculated and other relevant $\log\beta^0$ obtained from literatures were summarized in Table S2. Since MSWIA is typically produced by incineration of municipal solid waste at high temperature (~900–1100°C) under oxygenated environment [62], we assumed a negligible presence of low-valent metals (e.g., Cu^+, Fe^{2+}) in MSWIA.

3. Results and discussion

3.1. Metal extraction from MSWIA via citrate leaching

Details on the reaction procedure, characterization, and citrate leaching of MSWIA can be found in our previous study [12]. Major crystalline phases in MSWIA included calcium-, aluminum-, and magnesium-bearing carbonates and silicates. Microwave digestion of the MSWIA sample using aqua regia led to a quasi-complete matrix decomposition, with the only solid residue being a trace amount of transparent silicates. Since our previous study using synchrotron X-ray absorption spectroscopy (XAS) and microscopy elucidated that REE in MSWIA were primarily associated with phosphate minerals (e.g., xenotime) and iron oxides (e.g., hematite) [43], complete REE extraction from microwave digestion was assumed. The MSWIA sample contained 391 mg/kg of total REE, with particularly high Pr and Nd concentrations that was likely originated from electronic wastes. It also contained abundant non-REE, especially Mg, Al, Si, Ca, Fe, Cu, and Zn (Table S3). The metal leaching efficiency from MSWIA by citrate widely ranged from 20 to 98% (**Eq.** (1), which depends on the physical distribution and chemical speciation of these metals. Based on the metal concentrations in leachate (Table S3), we selected Al, Fe, Cu, Zn, and seven REE (Y, La, Ce, Pr, Nd, Gd, Dy) as our target metals for sequential recovery.

3.2. Metal pre-concentration via EFC

Prior to metal precipitation, EFC was employed to pre-concentrate metals in leachate. Note that determining the eutectic point of the leachate was not a focus of this study. In a preliminary test, EFC was performed on a 200 mL simulated solution containing 10 mmol/L $CaCl_2$ and 10 μmol/L YCl_3 at a freezing temperature of -20 °C. The solution temperature was decreased to around -4 °C within 540 min (Fig. S1**a**). Crystallized solid phase started to form at 0 °C and steadily grew, and the total volume of solid phase eventually reached ~212 cm^3 at 540 min with only ~21 mL of solution remained. The solution pH remained

relatively stable at 4.1–4.5 (Fig. S1**b**). Before 450 min, Ca^{2+} and Y^{3+} were well-retained in the aqueous phase (Fig. S1). After 450 min, however, the retained fractions of Ca^{2+} and Y^{3+} rapidly declined, indicating that the temperature was below the eutectic point and solutes were crystallized (Fig. S2). The similar profiles of Ca^{2+} and Y^{3+} suggested the indiscriminative concentration of solutes by EFC. Based on the preliminary results shown in Fig. 1, **450** min was the optimal freezing time, at which near 90% of Ca^{2+} and Y^{3+} were retained in the aqueous phase (**Eq.** (2), and their concentrations increased to more than seven-folded (**Eq.** (3). Note that since many organic compounds such as citric acid do not form a well-defined eutectic system like inorganic salts do, they tend to remain dissolved in water and become concentrated instead of crystallizing as solid phases.

EFC was then conducted on the real citrate leachate of MSWIA under the optimal conditions, and the corresponding characteristics of target metals in EFC concentrate were summarized in Table S4. Overall, the concentration profiles were similar to the simulated solution, with ~88–94% of target metals retained and a concentration factor of ~6.7–8.3. After EFC, the solution volume was reduced from 200 mL to ~20 mL, and the final pH was 4.1 ± 0.2. To determine the effect of pre-concentration, the EFC concentrate and the original leachate without EFC were both used as feedstocks for subsequent metal precipitation processes.

3.3. Recovery of Cu and Zn via sulfide precipitation

Sulfide precipitation is widely applied in hydrometallurgical treatment of ore leachates owing to the low solubility of certain metal sulfides, potential for selective removal, fast kinetics, and good settling properties [63]. Using sulfide could preferentially precipitate Cu^{2+} and Zn^{2+} from the leachate considering the particularly low solubility product constants (K_{sp}) of their sulfide products (7.9×10^{-37} for CuS and 2.0×10^{-25} for ZnS at 25 °C) compared to other metal ions in the leachate [34]. Thermodynamic modeling using PHREEQC was first performed to predict the metal–ligand interactions after sulfide is added, with measured solution chemistry of leachate and EFC concentrate as the input (Table S1). The results suggested complete complexation and precipitation of Cu^{2+} with sulfide to form $Cu(HS)_2^0$ for both leachate (without EFC) and EFC concentrate (with EFC) with a positive SI of 8.32 (Fig. 2**a-b**, Table 1). On the other hand, 77.5% of Zn^{2+} in leachate forms soluble citrate complex $Zn(C_6H_7O_7)^+$ due to the strong complexing ability between citrate and Zn^{2+} (Table S2), and only 15.8% complexes as $Zn(HS)_2^0$. Surprisingly, however, 95.6% of Zn^{2+} in EFC concentrate precipitates as $Zn(HS)_2^0$ (SI = 5.59), with only ~4% exists as free Zn^{2+}. The notably enhanced Zn precipitation in EFC concentrate can be attributed to the increased concentrations of Zn^{2+} and sulfide compared to leachate, which strongly favor complexation. In addition, complexation between other metals and sulfide was predicted to be negligible, and they predominantly complex with citrate. For example, ~99% of Fe^{3+} forms $Fe(C_6H_6O_7)^+$, whereas REE form both $REE(C_6H_6O_7)^+$ and $REE(C_6H_5O_7)^0$ (Table 1). Mg^{2+} and Ca^{2+} were two exceptions that mainly exist as free cations, possibly due to the low $\log\beta^0$ of their citrate complexes (Table S2).

In order to confirm the modeling results, batch experiments of sulfide precipitation were performed on leachate and EFC concentrate. The reaction time of 30 min was selected based on a preliminary kinetic experiment to achieve steady state (Fig. S3). Black precipitates formed immediately after sulfide was added to the solutions. Based on XRD analysis, the sulfide product of EFC concentrate consisted of 67.5% sphalerite (ZnS) and 32.5% covellite (CuS) (Fig. S4, Table S5). The SEM image showed the growth of irregularly-shaped particles on bigger aggregates (Fig. 3**a**, Fig. S5). The average particle size of individual sulfide particle was around 10–30 nm, and the size of aggregates typically ranged from 10–20 μm. In addition, emissions of Cu L_α (0.93 keV), K_α (8.04 keV), and K_β (8.91 keV) edges, Zn L_α (1.01 keV), K_α (8.63 keV), and K_β (9.57 keV), and S K_α (2.31 keV) and K_β (2.46 keV) edges were observed by EDX analysis (Fig. 3**b**).

The precipitation efficiencies of Cu^{2+} and Zn^{2+} in leachate were 88.2% and 9.69%, respectively (**Eq.** (4) (Fig. 2**c**), with the majority of Zn^{2+} remained in solution, whereas for EFC concentrate, 96.0% of Cu^{2+} and 90.9% of Zn^{2+} precipitated as sulfides (Fig. 2**d**). Precipitation of other metals were negligible. Weight percentages of Cu and Zn in sulfide product of EFC concentrate reached 16.6% and 40.2% (**Eq.** (5), respectively, with only 1.9% of metal impurity (mostly Ca and Fe) and the remaining fraction likely as S (Table S6). Pre-concentration by EFC increased the enrichment factor of Cu from 22.4 to 29.4 and Zn from 2.93 to 35.4 (**Eq.** (6), Fig. 4**a**). The Cu and Zn concentrations in sulfide product with pre-concentration were around 30 times higher than raw MSWIA. Furthermore, the overall recovery rates of 96.0% for Cu and 94.5% for Zn (**Eq.** (7) illustrated that Cu and Zn in the MSWIA sample were almost completely recovered by sulfide precipitation with a high product purity (Fig. 4**b**). In comparison, Cu and Zn only accounted for 12.6% and 3.33% of product mass for leachate, respectively, and the metal impurity was 5.28%. Only 9.68% of Zn in MSWIA was recovered. The experimental results agreed well with thermodynamic modeling, confirming the high selectivity of sulfide precipitation towards Cu^{2+} and Zn^{2+} and enhancive effect of pre-concentration.

To monitor the effect of pH on each metal precipitation process, the changes in major metal speciation at different solution pH were predicted by PHREEQC and presented in Table S7–S9. During sulfide precipitation, the precipitation efficiency of Cu is largely unaffected from pH 2–8, while that of Zn is slightly reduced as pH decreases to 2 (Table S7). Hydroxide starts to outcompete citrate for Al and Fe above neutral pH and forms insoluble Al- and Fe-hydroxides at pH 8. Other metals such as Mg, Ca, and REE remain soluble, either as free cations or citrate complexes. Overall, a moderately acidic condition (pH 4–6) is suitable for selective precipitation of Cu and Zn.

3.4. Recovery of Al and Fe via alkaline precipitation

The solubility of many metal species is pH-dependent, and they can precipitate as hydroxides under alkaline conditions, including Al^{3+}, Fe^{3+}, Cu^{2+}, and Zn^{2+} (Table S2). Now that Cu^{2+} and Zn^{2+} have been mostly recovered in EFC concentrate, the second precipitation process was designed to precipitate Al^{3+} and Fe^{3+} by increasing solution pH. PHREEQC modeling predicted that at pH 9, ~76% of Al^{3+} and ~49% of Fe^{3+} in leachate without EFC would precipitate as hydroxides, while the remaining fractions mostly form citrate complexes (Fig. 5**a**). Note that the majority of Zn^{2+} still remained in leachate, which would likely precipitate as ZnS as pH rises. On the other hand, for EFC concentrate, 99.8% of Al^{3+} would precipitate as $Al(OH)_3^0$ (SI = 8.73), and 90.8% of Fe^{3+} would precipitate as $Fe(OH)_3^0$ (SI = 6.55) (Table 1). The complexation between Al^{3+}/Fe^{3+} and hydroxide anions is promoted by the higher metal concentrations in EFC concentrate. At pH 9.0, citrate is fully deprotonated as $C_6H_5O_7^{3-}$ ($pK_{a3} = 6.4$) [36], which forms stronger complexes with many metals than $C_6H_6O_7^{2-}$ (Table S2). Hence, ~80 % of REE form citrate complexes at pH 4 [mostly as $REE(C_6H_6O_7)^+$], whereas at pH 9, REE completely complex with citrate as $REE(C_6H_5O_7)_2^{3-}$ and $REE(C_6H_5O_7)^0$ (Fig. 2**b** vs. Fig. 5**b**).

After alkaline precipitation experiment (reaction time of 60 min according to Fig. S6), yellow precipitates were collected from EFC concentrate, which were identified by XRD analysis as 85.7% of natroalunite [$NaAl_3(SO_4)_2(OH)_6$] and 14.3% of jahnsite [$NaMg_2Fe_3(PO_4)_4(OH)_2(H_2O)_8$] (Fig. S7, Table S5). SEM images revealed two types of major morphologies: round-edged particles and cubic particles (Fig. 3**c**, Fig. S8). The round-edged particles showed an average size of ~200 nm to 1 μm, whereas the cubic particles were around 600 nm in length. EDX spectra collected on both types of particles indicated similar elemental compositions (Fig. 3**d**, Fig. S9). Emission of Al K_α (1.49 keV), Fe L_α (0.71 keV), K_α (6.40 keV), and K_β (7.06 keV) edges were observed.

For leachate without EFC, the measured precipitation efficiencies of Al^{3+}, Fe^{3+}, and Zn^{2+} were 71.9%, 45.6%, and 90.6%, respectively

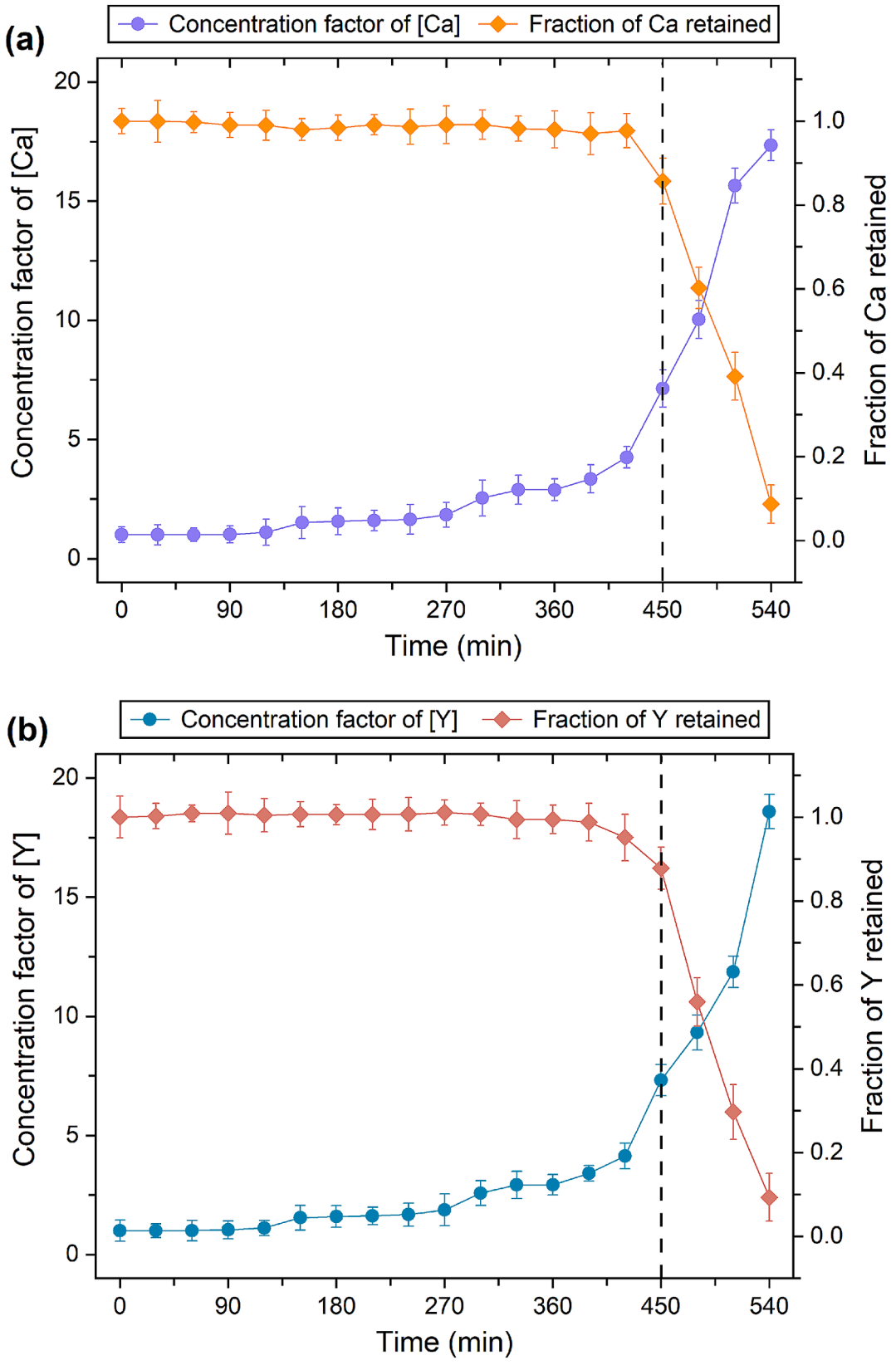

Fig. 1. The concentration factor and retained fraction of **(a)** Ca^{2+} and **(b)** Y^{3+} in the aqueous phase of a simulated solution during EFC (Freezing temperature: −20 °C; freezing time: 540 min; initial composition of simulated solution: 10 mmol/L $CaCl_2$ and 10 μmol/L YCl_3. Dashed lines indicated optimal freezing time at 450 min).

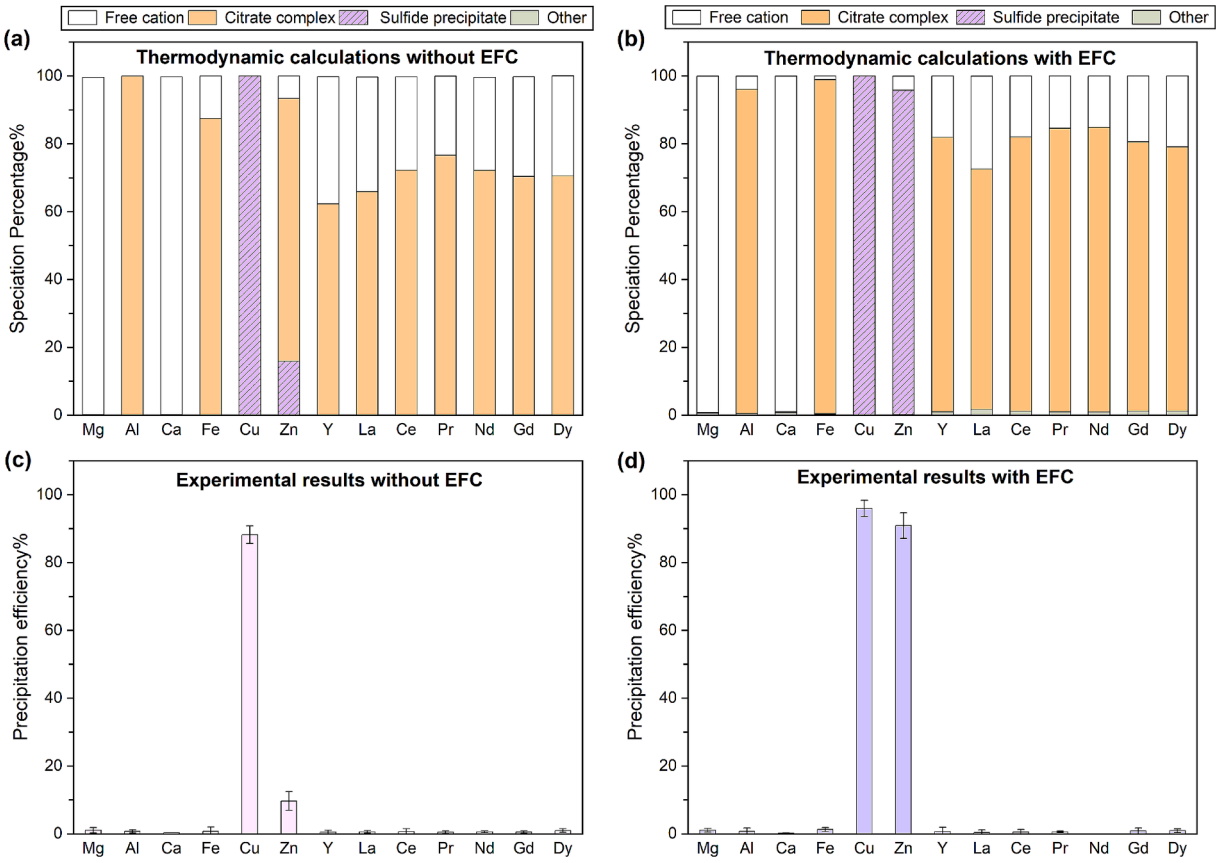

Fig. 2. (a-b) Thermodynamic calculations of metal speciation and **(c-d)** experimental results of metal precipitation efficiency during sulfide precipitation in leachate (without EFC) and EFC concentrate (with EFC). Reaction conditions: sulfide dosage = 15 mg; pH = 4.1 ± 0.2; reaction time = 30 min; temperature = 23 °C; pe = 4.

Table 1
Major metal species in EFC concentrate during each stage as predicted by PHREEQC using logβ^0 in **Table S2**.

Element	EFC Concentrate (pH 4)		Sulfide Precipitation (pH 4)		Alkaline Precipitation (pH 9)		Oxalate Precipitation (pH 9)	
	Major species	SI	Major species	SI	Major species	SI	Major species	SI
Mg	99.3% Mg^{2+}		99.2% Mg^{2+}		51.6% Mg^{2+}		54.6% $Mg(C_6H_5O_7)^-$	
	0.35% $Mg(C_6H_7O_7)^+$		0.57% $Mg(C_6H_6O_7)^0$		48.2% $Mg(C_6H_5O_7)^-$		41.6% Mg^{2+}	
Al	97.5% $Al(C_6H_6O_7)^+$		95.6% $Al(C_6H_6O_7)^+$		99.8% $Al(OH)_3^0$	8.73		
	2.46% Al^{3+}		3.91% Al^{3+}		0.19% $Al(C_6H_5O_7)^0$			
Ca	99.0% Ca^{2+}		99.0% Ca^{2+}		52.7% Ca^{2+}		64.6% $Ca(C_6H_5O_7)^-$	
	0.69% $CaSO_4^0$	−1.28	0.72% $Ca(C_6H_6O_7)^0$		47.0% $Ca(C_6H_5O_7)^-$		29.2% Ca^{2+}	
							5.38% $Ca(C_2O_4)^0$	4.24
Fe	92.6% $Fe(C_6H_6O_7)^+$		98.6% $Fe(C_6H_6O_7)^+$		90.8% $Fe(OH)_3^0$	6.55		
	6.47% Fe^{3+}		1.03% Fe^{3+}		6.37% $Fe(C_6H_5O_7)^0$			
Cu	83.1% $Cu(C_6H_7O_7)^+$		100% $Cu(HS)_2^0$	8.32				
	16.7% Cu^{2+}							
Zn	94.2% $Zn(C_6H_7O_7)^+$		95.6% $Zn(HS)_2^0$	5.59				
	5.82% Zn^{2+}		4.09% Zn^{2+}					
Y	79.2% $Y(C_6H_6O_7)^+$		81.0% $Y(C_6H_6O_7)^+$		98.8% $Y(C_6H_5O_7)^0$		99.6% $Y_2(C_2O_4)_3^0$	0.41
	19.9% Y^{3+}		18.1% Y^{3+}				0.33% $Y(C_6H_5O_7)^0$	
La	68.5% $La(C_6H_6O_7)^+$		70.9% $La(C_6H_6O_7)^+$		63.4% $La(C_6H_5O_7)_2^{3-}$		98.6% $La_2(C_2O_4)_3^0$	0.56
	31.5% La^{3+}		27.5% La^{3+}		36.2% $La(C_6H_5O_7)^0$		1.44% $La(C_6H_5O_7)_2^{3-}$	
Ce	79.0% $Ce(C_6H_6O_7)^+$		66.5% $Ce(C_6H_6O_7)^+$		68.3% $Ce(C_6H_5O_7)_2^{3-}$		99.2% $Ce_2(C_2O_4)_3^0$	0.63
	19.8% Ce^{3+}		18.0% Ce^{3+}		31.3% $Ce(C_6H_5O_7)^0$		0.77% $Ce(C_6H_5O_7)_2^{3-}$	
	0.87% $Ce(SO_4)^+$		14.4% $Ce(C_6H_5O_7)^0$					
Pr	81.9% $Pr(C_6H_6O_7)^+$		83.6% $Pr(C_6H_6O_7)^+$		99.5% $Pr(C_6H_5O_7)^0$		98.9% $Pr_2(C_2O_4)_3^0$	1.51
	17.1% Pr^{3+}		15.5% Pr^{3+}				1.08% $Pr(C_6H_5O_7)^0$	
Nd	82.2% $Nd(C_6H_6O_7)^+$		62.1% $Nd(C_6H_6O_7)^+$		51.2% $Nd(C_6H_5O_7)_2^{3-}$		98.6% $Nd_2(C_2O_4)_3^0$	2.80
	16.8% Nd^{3+}		21.8% $Nd(C_6H_5O_7)^0$		48.2% $Nd(C_6H_5O_7)^0$		1.33% $Nd(C_6H_5O_7)_2^{3-}$	
			15.2% Nd^{3+}					
Gd	67.8% $Gd(C_6H_6O_7)^+$		52.1% $Gd(C_6H_6O_7)^+$		56.7% $Gd(C_6H_5O_7)_2^{3-}$		99.3% $Gd_2(C_2O_4)_3^0$	0.33
	29.4% Gd^{3+}		27.3% $Gd(C_6H_5O_7)^0$		42.3% $Gd(C_6H_5O_7)^0$		0.65% $Gd(C_6H_5O_7)_2^{3-}$	
	2.63% $Gd(C_6H_5O_7)^0$		19.4% Gd^{3+}					
Dy	75.8% $Dy(C_6H_6O_7)^+$		54.5% $Dy(C_6H_6O_7)^+$		61.4% $Dy(C_6H_5O_7)_2^{3-}$		99.4% $Dy_2(C_2O_4)_3^0$	0.72
	12.9% $Dy(C_6H_5O_7)^0$		23.4% $Dy(C_6H_5O_7)^0$		36.6% $Dy(C_6H_5O_7)^0$		0.61% $Dy(C_6H_5O_7)_2^{3-}$	
	11.1% Dy^{3+}		20.9% Dy^{3+}					

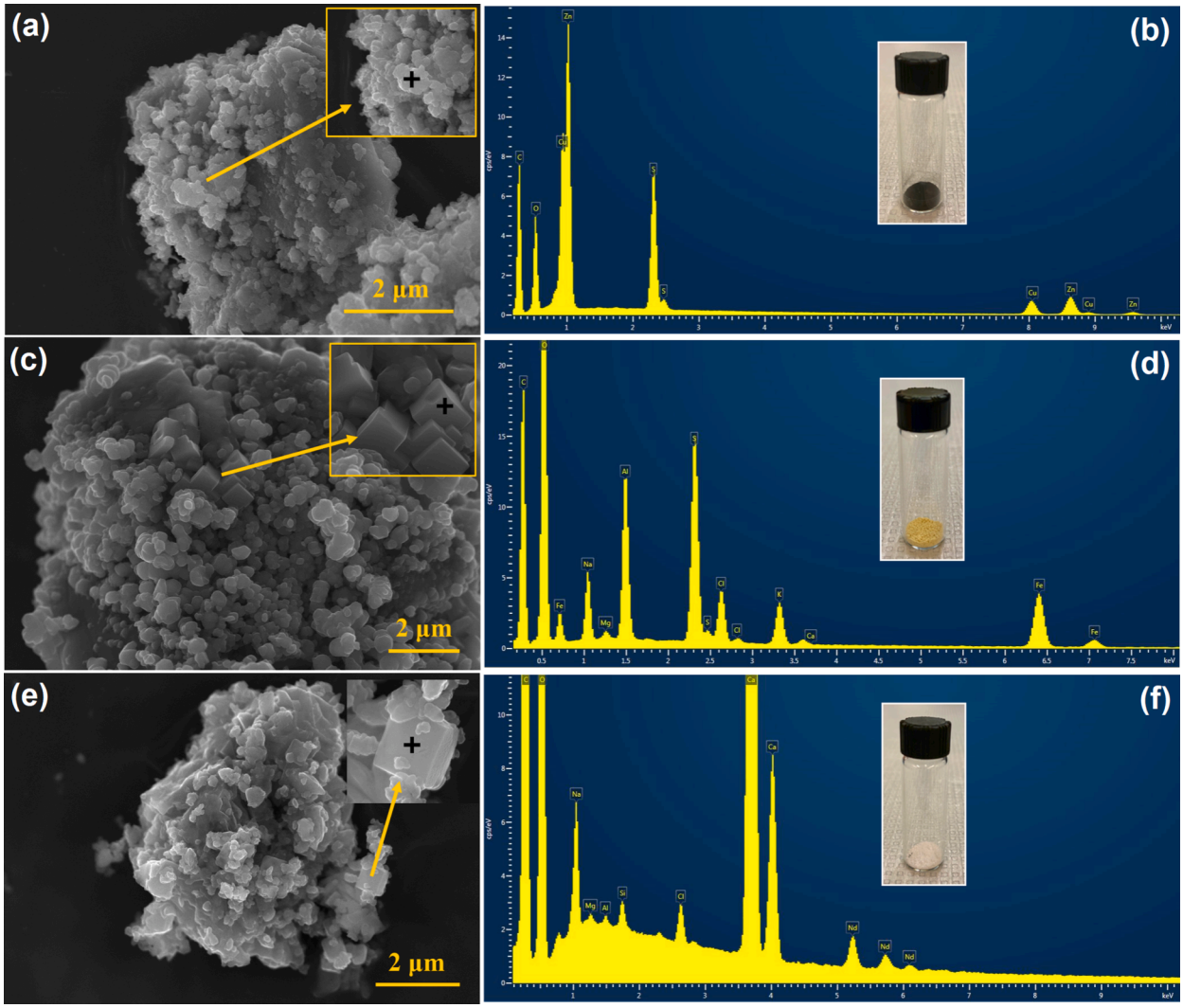

Fig. 3. SEM images and EDX spectra of solid products from: **(a-b)** sulfide precipitation, **(c-d)** alkaline precipitation, and **(g-h)** oxalate precipitation. Insets in SEM images are zoomed-in view. Black crosses denote selected points for EDX analyses. Insets in EDX spectra are pictures of solid products.

(Fig. 5**c**). The wt% of Al and Fe in the alkaline product were 25.0% and 12.3%, respectively, with an enrichment factor of ~3 (**Table S6**). Co-precipitation of ZnS led a higher metal impurity, and only 71.2 % of Al and 46.5 % of Fe in MSWIA were recovered (Fig. 4**b**). In contrast, precipitation of Al^{3+} (99.0%) and Fe^{3+} (97.1%) was highly effective for EFC concentrate (Fig. 5**d**). Al and Fe constituted 40.8% and 33.5% of product, respectively, with only ~1.5% of metal impurity (**Table S6**). The overall recovery rates of Al and Fe reached 98.9% and 97.0%, and corresponding enrichment factors were 5.71 and 9.07, respectively (Fig. 4). The experimental results of both solutions matched well with thermodynamic modeling. The effective removal of Cu^{2+} and Zn^{2+} from EFC concentrate via sulfide precipitation contributed to a higher Al and Fe purity in alkaline product.

As shown in **Table S8**, the precipitation efficiency of Al and Fe reaches the maximum at pH 9 and starts to drop as pH further increases due to the formation of soluble hydroxide complexes such as $Al(OH)_4^-$ and $Fe(OH)_4^-$. On the other hand, complexations between REE and hydroxide and carbonate become dominant as pH reaches 11, and REE start to precipitate as hydroxides. This indicates that pH 9 is optimal for the selective precipitation of Al and Fe.

3.5. Recovery of REE via oxalate precipitation

It has been inferred that co-precipitation of REE with Ca-oxalate (K_{sp} = 1.7 × 10^{-9} at 25 °C) via substitution is thermodynamically and kinetically favorable because of the similar ionic radii of Ca^{2+} (1.12 Å) and REE^{3+} (~0.99 to 1.16 Å) with an 8-fold coordination, high reaction equilibrium constant, and fast kinetics, and thus it is particularly suitable for REE recovery from Ca-rich feedstocks [12,14,64–66]. In this study, oxalate precipitation was designed as the last step to selectively recover REE. Since oxalate can form insoluble complexes with many metals including Al, Fe, Cu, and Zn (**Table S2**) [67], the prior two precipitation processes were performed to remove these metals first and to minimize the impurity in oxalate product. Based on thermodynamic modeling, ~70% of REE in leachate without EFC would co-precipitate with Ca-oxalate, and the remaining 30% complex with citrate (Fig. 6**a**). The Fe^{3+} that was not removed by alkaline precipitation would form insoluble $Fe_2(C_2O_4)_3^0$ (SI = 0.87). For EFC concentrate, however, ~100% of REE complex with oxalate to form insoluble $REE_2(C_2O_4)_3^0$, with a positive SI of 0.33–2.80 (Fig. 6**b**, Table 1). REE-oxalate complexes have high $\log\beta^0$ ranging from 5.9 to 6.8 for monodentate and 10.5–11.4 for bidentate complexes (**Table S2**). Around 5% of Ca^{2+} was predicted to precipitate as $Ca(C_2O_4)^0$ (SI = 4.24), which would be enough to co-precipitate REE considering the significantly higher Ca^{2+} concentration compared to REE (Table 1). In addition, 64.6% of Ca^{2+} forms $Ca(C_6H_5O_7)^-$, while the remaining 29.2 % exists as free Ca^{2+}.

Preliminary results indicated that REE rapidly precipitated as white precipitates within 20 min (**Fig. S10**). The XRD pattern suggested that

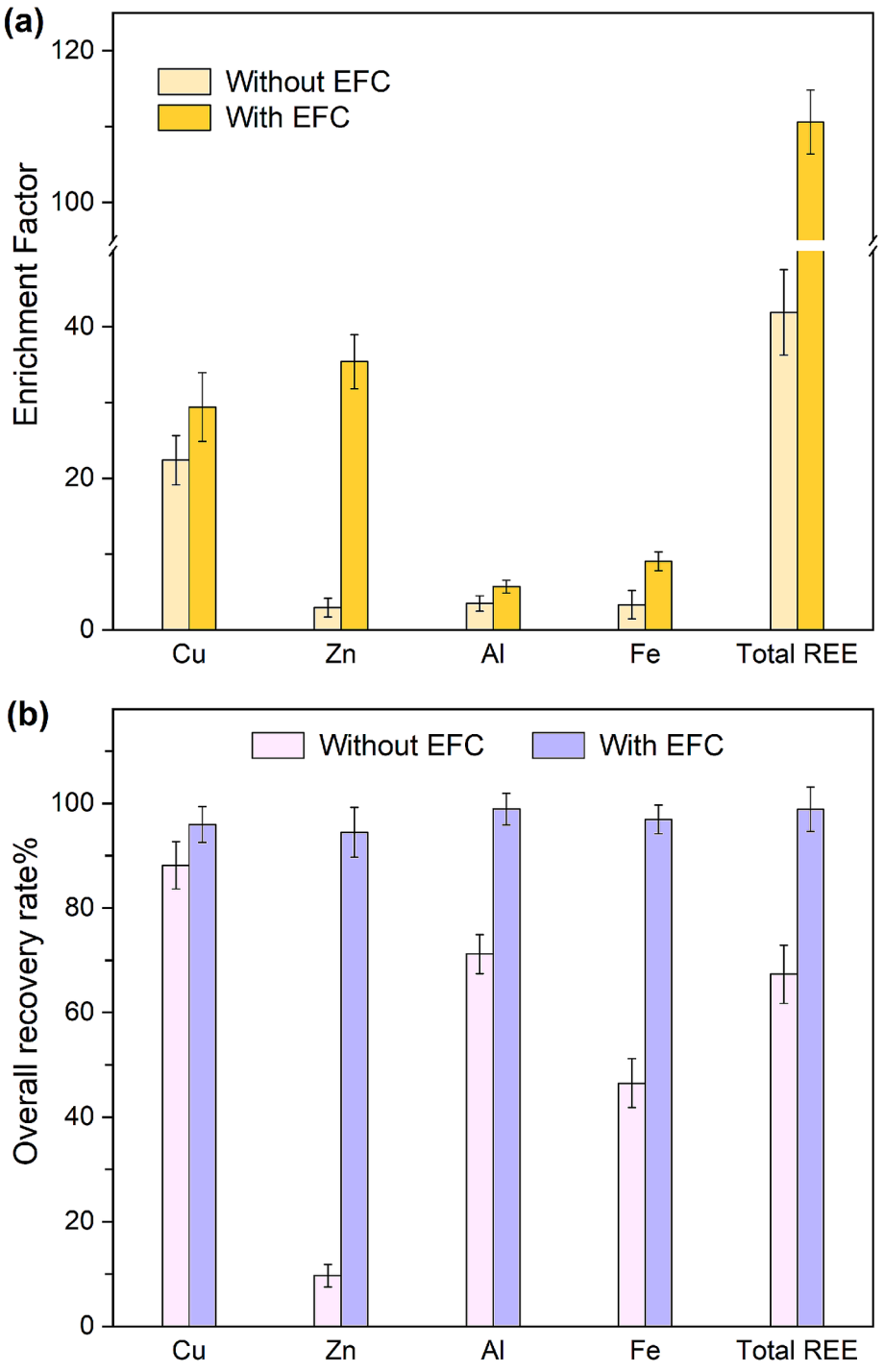

Fig. 4. **(a)** Enrichment factors of target metals in the precipitation products compared to raw MSWIA; **(b)** overall recovery.

oxalate product of EFC concentrate contained predominantly (>99%) weddellite [$Ca(C_2O_4)_2{\cdot}2H_2O$] (**Fig. S11**, **Table S5**). The weddellite particles appeared as near-rhombic shaped, though most of the particles did not have well-defined shapes or edges, probably due to incomplete nucleation and crystal growth within a short reaction time (Fig. 3**e**). The average size of rhombic-shaped individual weddellite particle was around 200–500 nm. The strong emission peaks of Ca K_α (3.69 keV) and K_β (4.01 keV) edges can be clearly observed from the EDX spectra, as well as the L_α (5.23 keV), $L_{\beta1}$ (5.72 keV), and $L_{\beta2}$ (6.09 keV) edges of Nd, the most concentrated REE (Fig. 3**f**).

The metal precipitation efficiencies followed a consistent pattern with the modeling results. Without EFC, 83.6% of Fe^{3+} and 68.2% of total REE in leachate precipitated (Fig. 6**c**). The weight percentage of total REE in oxalate product was 1.64% (**Table S6**). Ca-oxalate accounted for 84.2% of product mass, and co-precipitation of Fe^{3+} was responsible for a 12.3% of metal impurity. Around 67% of total REE was recovered from MSWIA, with an enrichment factor of ~40. For EFC concentrate, however, precipitation efficiencies of all seven REE were notably increased to >99%, along with ~3% precipitation of Ca^{2+} (Fig. 6**d**). The oxalate product contained 4.33 wt% of total REE and 94.5 wt% of Ca-oxalate, with only 1.26 wt% of metal impurity (**Table S6**). The wt% of Nd as the most concentrated REE in the oxalate product reached ~2.6%. About 99% of total REE from MSWIA was recovered, and significantly, the total REE concentration in oxalate product

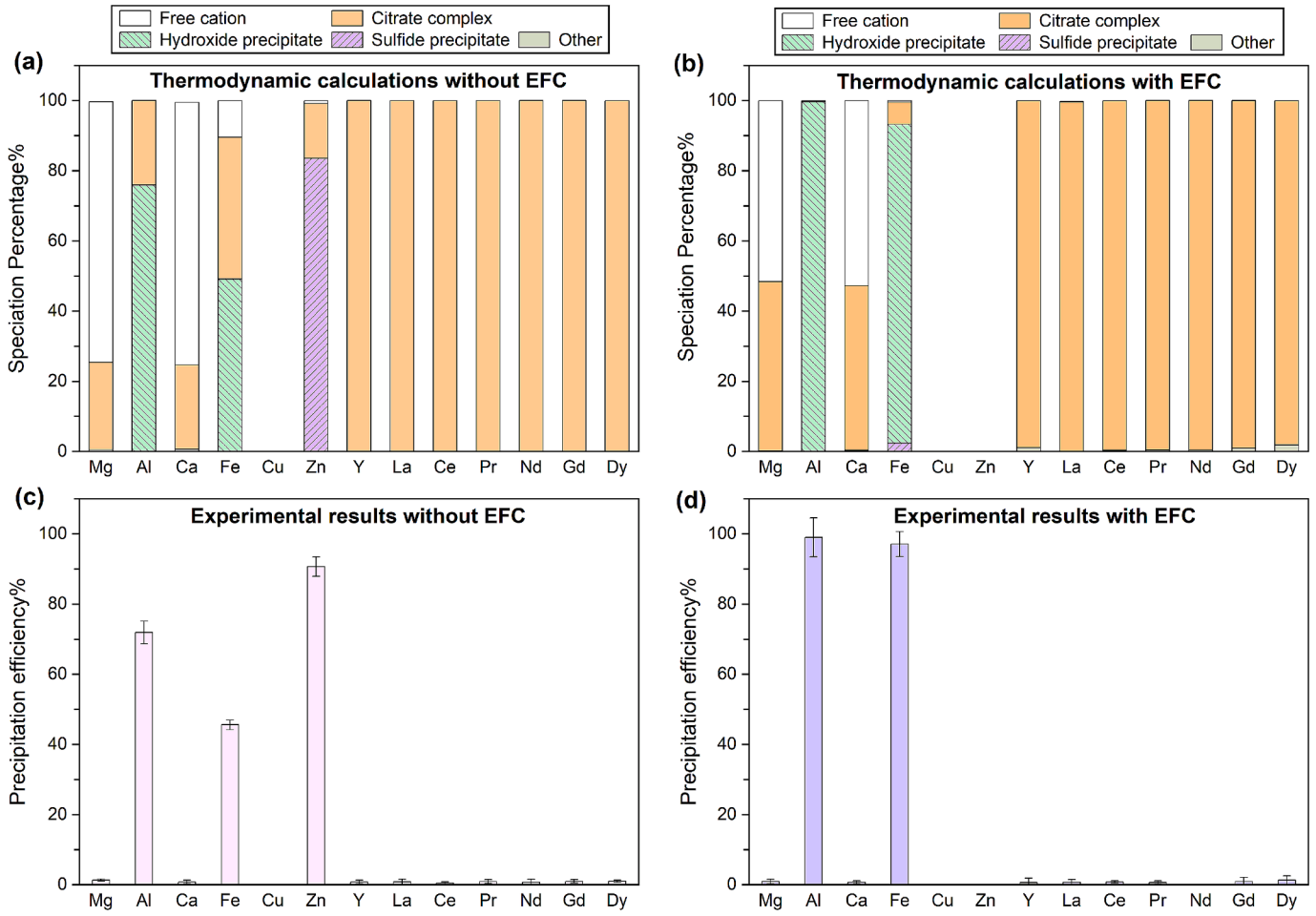

Fig. 5. (a-b) Thermodynamic calculations of metal speciation and **(c-d)** experimental results of metal precipitation efficiency during alkaline precipitation in leachate (without EFC) and EFC concentrate (with EFC). Metals that were mostly removed during sulfide precipitation were not shown here. Reaction conditions: pH = 9.0 ± 0.1; reaction time = 60 min; temperature = 23 °C; pe = 4.

(43,255 mg/kg) was ~110 times higher than raw MSWIA (390 mg/kg) and more than double of the oxalate product from leachate without EFC (16,407 mg/kg) (Fig. 4). The oxalate product of EFC concentrate contained almost purely of REE and Ca-oxalate, which can be either dissolved in acids or calcined to product REE/Ca-oxides. REE and Ca can be easily separated (e.g., ion exchange, solvent extraction), and oxalate can be recycled to reduce costs.

As pH increases from 8 to 11, the precipitation efficiencies of of REE remain unaffected because they are already near complete (**Table S9**). However, precipitation of Ca as oxalate steadily increases, and ~30% of Mg precipitates as oxalate at pH 11. Hence, pH 8 allows effectively recovery of REE while minimizing the amount of Ca and Mg as impurities in the oxalate product.

3.6. Impacts of organic acids vs. mineral acids on metal precipitation

For comparison, the leaching efficiency and normalized leaching rate of target metals from MSWIA by 50 mmol/L of citric acid and hydrochloric acid were summarized in **Table S10**, respectively. With a relatively low acid concentration, hydrochloric acid showed a lower leaching efficiency and normalized leaching rate for target metals from MSWIA compared to citric acid, especially for Al, Ca, Zn, and several REE (e.g., Y, La, Pr). This is likely because metal leaching by inorganic acids mainly relies on a proton-assisted mechanism that requires an extremely acidic condition, while organic acids can dissolve metals via a ligand-assisted mechanism by forming soluble metal–ligand complexes [33,68]. We also point out that the metal leaching efficiency of inorganic and organic acids can vary depending on many factors (e.g., mineralogy of feedstocks, chemical speciation of metals) [69–72]. More efforts are needed to comprehensively compare the efficiency of inorganic acids vs. organic acids in metal leaching.

The presence of leaching ligands in leachate could still interact with metal cations and compete with precipitating ligands, yet their potential impacts on subsequent metal precipitation processes have been largely overlooked. As is shown in Table 1, metals in EFC concentrate are predominantly complexed with citrate (except Mg and Ca), including 83.1% Cu as $Cu(C_6H_7O_7)^+$ and 94.2% Zn as $Zn(C_6H_7O_7)^+$. During sulfide precipitation, sulfide outcompetes citrate for Cu and Zn and forms insoluble sulfide complexes due to higher $\log\beta^0$ [e.g., 17.3 for $Cu(HS)_2^0$ vs. 13.2 for $Cu(C_6H_7O_7)^+$, **Table S2**], whereas other metals mostly remain as citrate complexes. Similarly, as pH increases during alkaline precipitation, formation of insoluble $Al(OH)_3^0$ and $Fe(OH)_3^0$ becomes thermodynamically more favorable than $Al(C_6H_5O_7)^0$ and $Fe(C_6H_5O_7)^0$. The strong complexing ability of citrate with REE [$\log\beta^0$ of 9.4–10.4 for $REE(C_6H_5O_7)^0$ and $REE(C_6H_5O_7)_2^{3-}$] prevents them from complexing with sulfide and hydroxide ($\log\beta^0$ of ~3.8–8.2) until they form stronger oxalate complexes [$\log\beta^0$ of 10.7–12.9 for $REE_2(C_2O_4)_3^0$] in the last step. Our results revealed that presence of citrate serves as a protecting ligand for certain metals and played a key role in sequential metal recovery in this method.

In comparison, thermodynamic modeling was also performed to examine the metal–ligand interaction during precipitation processes under the same condition (assuming similar solution chemistry as the citrate EFC concentrate) using HCl or H_2SO_4 as the leaching agent, both

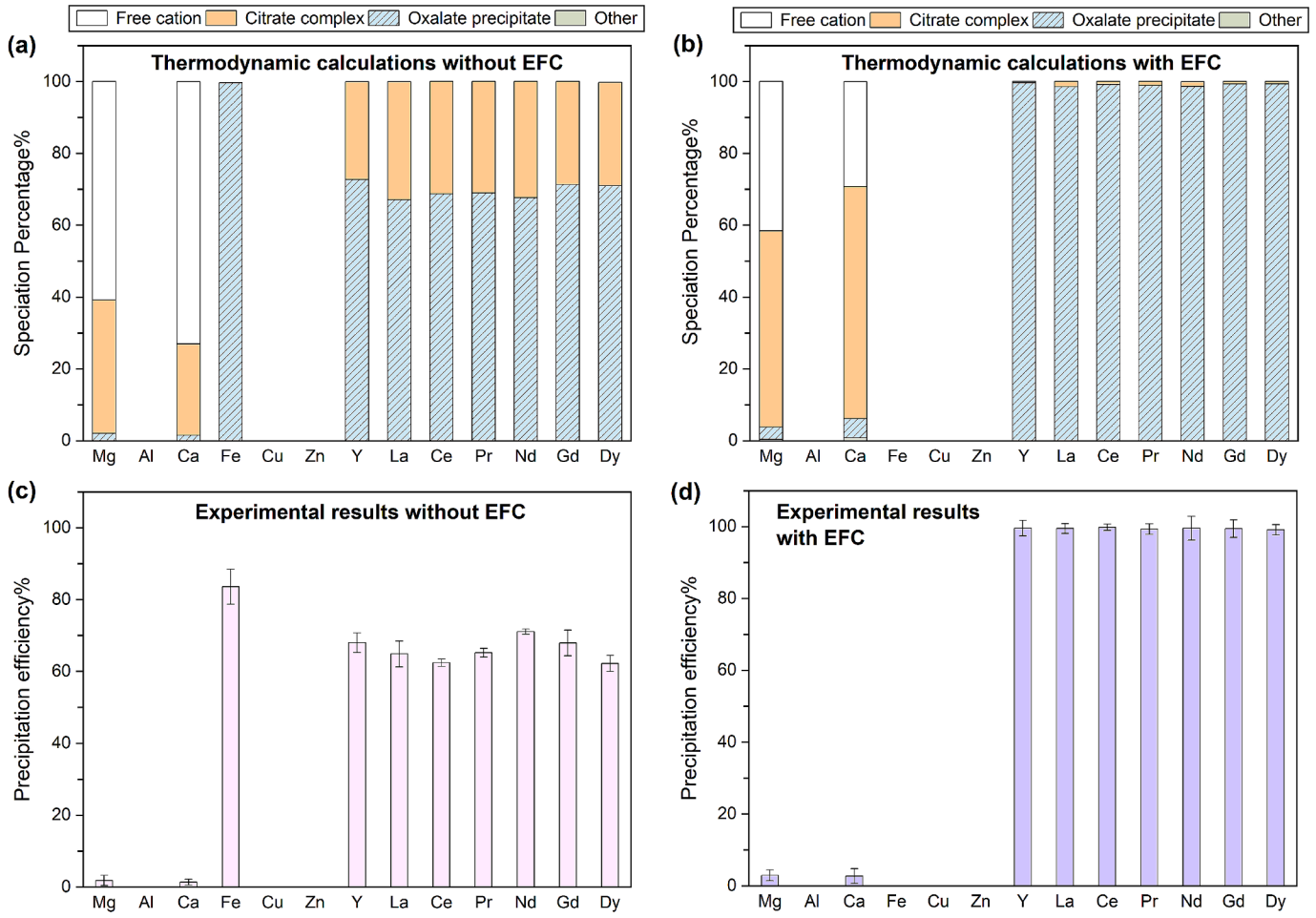

Fig. 6. **(a-b)** Thermodynamic calculations of metal speciation and **(c-d)** experimental results of metal precipitation efficiency during oxalate precipitation in leachate (without EFC) and EFC concentrate (with EFC). Metals that were mostly removed during sulfide precipitation were not shown here. Unshaded and shaded columns indicated soluble and insoluble phases, respectively; oxalate dosage = 10 mg; pH = 9.0 ± 0.1; reaction time: 20 min; temperature = 23 °C; pe = 4.

of which are commonly used in hydrometallurgy but have weaker metal complexing ability than citrate (Table S2). With HCl, near-complete precipitation of Cu^{2+} and Zn^{2+} can be achieved during sulfide precipitation (Fig. S12**a**). However, other target metals are predominantly present as free cations owing to the weak complexing ability of Cl^- ($log\beta^0$ of -0.89–2.13, Table S2). Consequently, hydroxide and carbonate dominate REE complexation ($log\beta^0$ of 2.32–12.9) as pH increases to 9 during alkaline precipitation, resulting in undesired co-precipitation of REE-hydroxides/carbonates mixed with Al-hydroxide and Fe-hydroxide/sulfide (Fig. S12**b**). Similar results are predicted for H_2SO_4, except for the lower REE precipitation rates during alkaline precipitation (Fig. S12**c-d**). This is likely due to the slightly stronger complexing ability of SO_4^{2-} ($log\beta^0$ of 3.48–5.20), which protects REE more effectively than Cl^-. In addition, phosphate is another inorganic ligand present in the leachate that could form insoluble complexes with many metals such as Ca, Fe, and Zn. However, formation of metal-phosphate complexes is thermodynamically less favorable than that of other metal–ligand complexes involved in each precipitation process (e.g., Cu-/Zn-sulfide, Al-/Fe-hydroxide, REE-oxalate) (Table S2). Our modeling results showed that the influence of phosphate on selective metal precipitation in this system is negligible.

From an economic perspective, the unit price of citric acid on the global market (~$600–900 per metric ton) is higher than those of other mineral acids such as HCl, H_2SO_4, and HNO_3 (~$100–300 per metric ton) that are commonly used in conventional hydrometallurgy. However, a much lower chemical input is required for citric acid (50 mmol/L in this study) to achieve a similar leaching efficiency with mineral acids (typically ~1–5 mol/L) owing to its strong metal-complexing abilities [73,74]. Further efforts are needed to evaluate the technoeconomic feasibility and life-cycle-impacts of using organic acids in REE recovery as compared to mineral acids.

3.7. Utilization and post-treatment of byproducts

In addition to the recovered metal products, this treatment method also produces three byproducts: MSWIA residue, EFC-crystallized water, and oxalate filtrate (Scheme 1). The MSWIA residue was still rich in Na, Mg, Al, Si, and Ca (Table S11), and can be used to synthesize zeolite, which can immobilize heavy metals in MSWIA and serve as a less-hazardous alternative for waste storage/disposal [12]. The EFC-crystallized water was relatively "clean" and thus can be either discharged as wastewater or reused after simple treatments (Table S11). The few metals with notable concentrations (~1–50 mg/kg) in the crystallized water can be easily removed by conventional water treatment processes. For example, Mg^{2+} and Ca^{2+} can be removed by softening processes (e.g., ion exchange, lime-soda precipitation), whereas Al^{3+}, Fe^{3+}, Cu^{2+}, and Zn^{2+} can be removed via coagulation and flocculation.

Since the oxalate filtrate contained particularly high concentrations of Mg^{2+} and Ca^{2+} (Table S11), it can be considered as a potential feedstock for CO_2 mineralization similarly to desalination brines [75]. Mg^{2+} and Ca^{2+} can react with bicarbonate/carbonate speciated from dissolved CO_2 to produce insoluble carbonate minerals with a reaction rate constant of $>10^6\ M^{-1}{\cdot}s^{-1}$ [76]. Based on reaction stoichiometry and

assuming a 90% extent of reaction, oxalate filtrate produced from 1 g of MSWIA can sequester 0.27 g of CO_2, and thus a total of ~2.1 million tons of CO_2 can be sequestered if all 8 million tons of annually produced MSWIA in the U.S. is recycled using this method, which requires further studies to confirm [77].

4. Environmental implications

In this study, we demonstrated intensified and sequential recovery of REE and four other valuable metals (Al, Fe, Cu, Zn) from leachate of an incineration byproduct using combined physical concentration and sequential chemical precipitation processes. This modular process is expected to be applicable not only to MSWIA, but also other feedstocks containing these target metals (e.g., coal ash, mine tailings, electronic wastes). The effectiveness and feasibility of this process were substantiated by experimental data and thermodynamic modeling results. EFC as an example of pre-concentration method effectively enriched target metals in the leachate by ~7–8 times and remarkably improved the precipitation efficiency, product purity, and overall recovery rate of target metals. With EFC, 96.0% of Cu, 94.5% of Zn, 98.9% of Al, 97.0% of Fe, and 98.9% of total REE were selectively recovered by the three precipitation processes, with >98 % overall product purity. Compared to raw MSWIA, this recovery system enriched Cu and Zn by ~30 times, Al and Fe by ~6–9 times, and total REE by ~110 times in the purified products. The mineralogy, morphology, and elemental composition of these solid products were characterized and confirmed by XRD, SEM, and EDS. A ten-fold reduction in leachate volume by EFC is also favorable for downstream processing. According to thermodynamic modeling, the enhancive effect of pre-concentration can be mainly ascribed to the enhanced metal–ligand complexation between target metals and precipitating ligands at a higher solute concentration. Note that this work exemplified the feasibility of EFC in metal pre-concentration and selective recovery. However, the freezing temperature and freezing time of this process can be further optimized to improve the overall processing efficiency, which requires additional investigation. The energy consumption of EFC can be further reduced or even completely offset if climate-driven refrigeration can be utilized [29]. Continuously stirred reactors or continuously flowing pipelines can be installed in cold regions to allow spontaneous crystallization of water and constant mobilization and removal of floating ice phase. Note that pre-concentration can also be achieved using other techniques (e.g., forward osmosis membrane) [78], but corresponding energy consumption and effectiveness need to be evaluated.

Although organic acids have been studied as greener alternatives to mineral acids in hydrometallurgical processes owing to the ligand-promoted dissolution mechanism, previous studies considered them solely as leaching agents [79–81]. Comparisons between organic and mineral acids have been mainly focused on their metal leaching efficiency [82,83], but their influence on subsequent metal separation processes (especially chemical precipitation) has been overlooked. Our results showed that presence of citrate in leachate strongly governs metal–ligand complexation during metal precipitation processes and their selectivity/efficiency. Mineral acids with weak metal complexing ability tend to have minor impacts on metal–ligand interactions and thus are not ideal for selective metal recovery via chemical precipitation, whereas organic ligands with strong metal complexing ability can prevent premature precipitation of target metals and allow effective precipitation at the designated step. A suitable organic ligand can serve as both a leaching agent for metal extraction as well as protecting agent during metal precipitation, which is crucial for selective metal recovery. This study exemplifies the feasibility of an organic ligand-based treatment method for sequential recovery of multiple critical metals. To date, the performance of mineral and organic acids in hydrometallurgy is still controversial, and our results suggested that future evaluation needs to consider the influence of these ligands on the overall metal recovery process instead of solely on metal extraction.

CRediT authorship contribution statement

Yinghao Wen: Writing – review & editing, Writing – original draft, Visualization, Validation, Methodology, Investigation, Formal analysis. **Emily L. Tribby:** Investigation. **Yuanzhi Tang:** Writing – review & editing, Supervision, Resources, Project administration, Methodology, Investigation, Funding acquisition, Conceptualization.

Declaration of competing interest

The authors declare that they have no known competing financial interests or personal relationships that could have appeared to influence the work reported in this paper.

Acknowledgements

This work was supported by the Department of Energy ARPA-E Grant #DE-AR0001394 and National Science Foundation Grant # 2327660. We acknowledge Simin Zhao for assistance with ICP-MS set up and measurements. A portion of the analyses was performed at the Georgia Tech Institute for Electronics and Nanotechnology (IEN), a member of the National Nanotechnology Coordinated Infrastructure (NNCI), which is supported by the National Science Foundation (Grant ECCS-2025462).

Appendix A. Supplementary data

The Supplementary Material is available free of charge at: Chemicals and reagents, sample processing and characterizations, input of solution chemistry for PHREEQC modeling, stability constants of relevant metal-ligand complexes, elemental compositions and leaching characteristics of MSWIA, EFC characteristics of a simulated solution, phase diagram of a eutectic process, characteristics of target metals during EFC, decay in target metal concentrations during precipitation processes, PHREEQC modeling results of metal speciation at different pH during precipitation processes, XRD patterns of precipitation products and reference patterns of major phases, mineralogy of precipitation products, SEM images and EDX spectra of precipitation products, leaching characteristics of target metals by citric acid and hydrochloric acid, PHREEQC modeling results of metal speciation with HCl and H_2SO_4, elemental compositions of byproducts. Supplementary data to this article can be found online at https://doi.org/10.1016/j.cej.2025.162661.

Data availability

Data will be made available on request.

References

[1] H. Prommer, Towards sustainable rare-earth-element mining, Nat. Sustainability 6 (1) (2023) 13–14.
[2] R. Pell, L. Tijsseling, K. Goodenough, F. Wall, Q. Dehaine, A. Grant, D. Deak, X. Yan, P. Whattoff, Towards sustainable extraction of technology materials through integrated approaches, Nat. Rev. Earth Environ. 2 (10) (2021) 665–679.
[3] X. Du, T.E. Graedel, Global in-use stocks of the rare earth elements: a first estimate, Environ. Sci. Tech. 45 (9) (2011) 4096–4101.
[4] S. Massari, M. Ruberti, Rare earth elements as critical raw materials: Focus on international markets and future strategies, Resour. Policy 38 (1) (2013) 36–43.
[5] D.H. Dang, K.A. Thompson, L. Ma, H.Q. Nguyen, S.T. Luu, M.T.N. Duong, A. Kernaghan, Toward the circular economy of Rare Earth Elements: a review of abundance, extraction, applications, and environmental impacts, Arch. Environ. Contam. Toxicol. 81 (4) (2021) 521–530.
[6] F. Xie, T.A. Zhang, D. Dreisinger, F. Doyle, A critical review on solvent extraction of rare earths from aqueous solutions, Miner. Eng. 56 (2014) 10–28.
[7] G.-J.-P. Deblonde, A. Chagnes, G. Cote, Recent advances in the chemistry of hydrometallurgical methods, Sep. Purif. Rev. 52 (3) (2023) 221–241.
[8] E. Vahidi, F. Zhao, Environmental life cycle assessment on the separation of rare earth oxides through solvent extraction, J. Environ. Manage. 203 (2017) 255–263.
[9] J.C. Lee, Z. Wen, Pathways for greening the supply of rare earth elements in China, Nat. Sustainability 1 (10) (2018) 598–605.
[10] A. Amato, A. Becci, I. Birloaga, I. De Michelis, F. Ferella, V. Innocenzi, N. M. Ippolito, C.P.J. Gomez, F. Vegliò, F. Beolchini, Sustainability analysis of

innovative technologies for the rare earth elements recovery, Renew. Sustain. Energy Rev. 106 (2019) 41–53.
[11] R.K. Jyothi, T. Thenepalli, J.W. Ahn, P.K. Parhi, K.W. Chung, J.-Y. Lee, Review of rare earth elements recovery from secondary resources for clean energy technologies: grand opportunities to create wealth from waste, J. Clean. Prod. 267 (2020) 122048.
[12] Y. Wen, L. Hu, A. Boxleiter, D. Li, Y. Tang, Rare earth elements recovery and waste management of municipal solid waste incineration ash, ACS Sustainable Resource Management 1 (1) (2023) 17–27.
[13] S.M. Jowitt, T.T. Werner, Z. Weng, G.M. Mudd, Recycling of the rare earth elements, Curr. Opin. Green Sustainable Chem. 13 (2018) 1–7.
[14] P. Liu, S. Zhao, N. Xie, L. Yang, Q. Wang, Y. Wen, H. Chen, Y. Tang, Green approach for rare earth element (REE) recovery from coal fly ash, Environ. Sci. Tech. 57 (13) (2023) 5414–5423.
[15] F. Zhou, Y. Xiao, M. Guo, Y. Tang, W. Zhang, R. Qiu, Selective leaching of rare earth elements from ion-adsorption rare earth tailings: a synergy between CeO_2 reduction and Fe/Mn stabilization, Environ. Sci. Tech. 55 (16) (2021) 11328–11337.
[16] Q. Tan, J. Li, X. Zeng, Rare earth elements recovery from waste fluorescent lamps: a review, Crit. Rev. Environ. Sci. Technol. 45 (7) (2015) 749–776.
[17] C. Liu, Q. Yan, X. Zhang, L. Lei, C. Xiao, Efficient recovery of end-of-life NdFeB permanent magnets by selective leaching with deep eutectic solvents, Environ. Sci. Tech. 54 (16) (2020) 10370–10379.
[18] V.G. Deshmane, S.Z. Islam, R.R. Bhave, Selective recovery of rare earth elements from a wide range of e-waste and process scalability of membrane solvent extraction, Environ. Sci. Tech. 54 (1) (2019) 550–558.
[19] L. Stoy, V. Diaz, C.-H. Huang, Preferential recovery of rare-earth elements from coal fly ash using a recyclable ionic liquid, Environ. Sci. Tech. 55 (13) (2021) 9209–9220.
[20] A. Ding, C. Liu, X. Zhang, L. Lei, C. Xiao, ZnCl2: a green brønsted acid for selectively recovering rare earth elements from spent NdFeB permanent magnets, Environ. Sci. Tech. 56 (7) (2022) 4404–4412.
[21] R.C. Smith, R.K. Taggart, J.C. Hower, M.R. Wiesner, H. Hsu-Kim, Selective recovery of rare earth elements from coal fly ash leachates using liquid membrane processes, Environ. Sci. Tech. 53 (8) (2019) 4490–4499.
[22] Y. Zhang, J. Yan, J. Xu, C. Tian, K. Matyjaszewski, R.D. Tilton, G.V. Lowry, Phosphate polymer nanogel for selective and efficient rare earth element recovery, Environ. Sci. Tech. 55 (18) (2021) 12549–12560.
[23] L.N. Viana, A.P.S. Soares, D.L. Guimarães, W.J.S. Rojano, T.D. Saint'Pierre, Fluorescent lamps: a review on environmental concerns and current recycling perspectives highlighting Hg and rare earth elements, J. Environ. Chem. Eng. 10 (6) (2022) 108915.
[24] R. Eggert, C. Wadia, C. Anderson, D. Bauer, F. Fields, L. Meinert, P. Taylor, Rare earths: market disruption, innovation, and global supply chains, Annu. Rev. Env. Resour. 41 (2016) 199–222.
[25] P. Liu, R. Huang, Y. Tang, Comprehensive understandings of rare earth element (REE) speciation in coal fly ashes and implication for REE extractability, Environ. Sci. Tech. 53 (9) (2019) 5369–5377.
[26] F. Xu, S. Qin, S. Li, J. Wang, Q. Lu, J. Xing, Distribution, occurrence mode, and extraction potential of critical elements in coal ashes of the Chongqing Power Plant, J. Clean. Prod. 342 (2022) 130910.
[27] B. Fu, J.C. Hower, W. Zhang, G. Luo, H. Hu, H. Yao, A review of rare earth elements and yttrium in coal ash: content, modes of occurrences, combustion behavior, and extraction methods, Prog. Energy Combust. Sci. 88 (2022) 100954.
[28] D. Randall, J. Nathoo, A. Lewis, A case study for treating a reverse osmosis brine using Eutectic Freeze Crystallization—approaching a zero waste process, Desalination 266 (1–3) (2011) 256–262.
[29] G. Kolliopoulos, C. Xu, J.T. Martin, N. Devaere, V.G. Papangelakis, Hybrid forward osmosis-freeze concentration: a promising future in the desalination of effluents in cold regions, J. Water Process Eng. 47 (2022) 102711.
[30] F. Wu, X. Liu, G. Qu, P. Ning, A critical review on extraction of valuable metals from solid waste, Sep. Purif. Technol. 122043 (2022).
[31] S. Wu, L. Wang, L. Zhao, P. Zhang, H. El-Shall, B. Moudgil, X. Huang, L. Zhang, Recovery of rare earth elements from phosphate rock by hydrometallurgical processes–a critical review, Chem. Eng. J. 335 (2018) 774–800.
[32] B. Deng, X. Wang, D.X. Luong, R.A. Carter, Z. Wang, M.B. Tomson, J.M. Tour, Rare earth elements from waste, Sci. Adv. 8 (6) (2022) eabm3132.
[33] G. Furrer, W. Stumm, The coordination chemistry of weathering: I. Dissolution kinetics of δ-Al_2O_3 and BeO, Geochim. Cosmochim. Acta 50 (9) (1986) 1847–1860.
[34] NIST Critically Selected Stability Constants of Metal Complexes: Version 8.0, NIST, 2004.
[35] Y. Wen, P. Liu, Q. Wang, S. Zhao, Y. Tang, Organic ligand-mediated dissolution and fractionation of rare-earth elements (REEs) from carbonate and phosphate minerals, ACS Earth and Space Chemistry (2024).
[36] K. Burdzy, A. Aurich, S. Hunger, R. Jastrząb, M. Zabiszak, D. Kołodyńska, Green citric acid in the sorption process of rare earth elements, Chem. Eng. J. 437 (2022) 135366.
[37] J. Pan, B.V. Hassas, M. Rezaee, C. Zhou, S.V. Pisupati, Recovery of rare earth elements from coal fly ash through sequential chemical roasting, water leaching, and acid leaching processes, J. Clean. Prod. 284 (2021) 124725.
[38] B.V. Hassas, Y. Shekarian, M. Rezaee, Selective precipitation of rare earth and critical elements from acid mine drainage-part I: kinetics and thermodynamics of staged precipitation process, Resour. Conserv. Recycl. 188 (2023) 106654.
[39] P. Liu, Q. Wang, H. Jung, Y. Tang, Speciation, DISTRIBUTION, AND MOBILITY OF HAZARDOUS TRACE ELEMENTS IN COAL FLY ASH: INSIGHTS FROM Cr, Ni, and Cu, Energy Fuels 34 (11) (2020) 14333–14343, https://doi.org/10.1021/acs.energyfuels.0c02164.
[40] P. Liu, L.F. Yang, Q. Wang, B. Wan, Q. Ma, H.L. Chen, Y.Z. Tang, Speciation transformation of rare earth elements (REEs) during heating and implications for REE behaviors during coal combustion, Int. J. Coal Geol. 219 (2020), https://doi.org/10.1016/j.coal.2019.103371.
[41] E. Garcia, P. Liu, S.E. Bone, Y. Wen, Y. Tang, Systematic characterization of selenium speciation in coal fly ash, Environ. Sci. Processes Impacts 26 (12) (2024) 2240–2249, https://doi.org/10.1039/D4EM00398E.
[42] E. Garcia, P. Liu, J. Sanchez, S. Lee, Q. Wang, Y. Wen, S. Shivaprakash, S. Burns, Y. Tang, A survey study on arsenic speciation in coal fly ash and insights into the role of coal combustion conditions, Appl. Geochem. 170 (2024) 106095, https://doi.org/10.1016/j.apgeochem.2024.106095.
[43] Y. Wen, L. Hu, P. Liu, Q. Wang, E. Garcia, W. Yan, Y. Tang, Rare earth element (REE) speciation in municipal solid waste incineration ash, Appl. Geochem. 178 (2025) 106239.
[44] Y. Wen, P. Liu, Q. Wang, S. Zhao, Y. Tang, Organic ligand-mediated dissolution and fractionation of rare-earth elements (REEs) from carbonate and phosphate minerals, ACS Earth Space Chem. 8 (5) (2024) 1048–1061, https://doi.org/10.1021/acsearthspacechem.4c00009.
[45] D.D.G. Tokgoz, N.G. Ozerkan, S.J. Antony, Untreated municipal solid waste incineration ashes for cement replacement, Journal of Engineering Research 11 (3) (2023) 34–39.
[46] H. Waki, J. Fritz, The effect of organic solvents on complexes and ion exchange—II nitrate complexes of some divalent metals in isopropyl alcohol, J. Inorg. Nucl. Chem. 28 (2) (1966) 577–589.
[47] B. Mountain, T.M. Seward, Hydrosulfide/sulfide complexes of copper (I): experimental confirmation of the stoichiometry and stability of $Cu(HS)_2^-$ to elevated temperatures, Geochim. Cosmochim. Acta 67 (16) (2003) 3005–3014.
[48] J.P. Larentzos, L.J. Criscenti, A molecular dynamics study of alkaline earth metal–chloride complexation in aqueous solution, J. Phys. Chem. B 112 (45) (2008) 14243–14250.
[49] H. Irving, R. Williams, 637. The stability of transition-metal complexes, Journal of the Chemical Society (Resumed) (1953) 3192–3210.
[50] S. Andersson, K. Eberhardt, C. Ekberg, J.-O. Liljenzin, M. Nilsson, G. Skarnemark, Determination of stability constants of lanthanide nitrate complex formation using a solvent extraction technique, Radiochim. Acta 94 (8) (2006) 469–474.
[51] B.R. Tagirov, I.I. Diakonov, O.A. Devina, A.V. Zotov, Standard ferric–ferrous potential and stability of $FeCl_2^+$ to 90° C. Thermodynamic properties of $Fe^{3+}_{(aq)}$ and ferric-chloride species, Chem. Geol. 162 (3–4) (2000) 193–219.
[52] S. Stepanchikova, R. Biteikina, G. Shironosova, G. Kolonin, An experimental study of hydroxo complex formation in basic and near-neutral solutions of rare-earth elements and yttrium at 25 °C, Russ. Geol. Geophys. 55 (8) (2014) 941–944.
[53] R.P. Singh, Y.D. Yeboah, E.R. Pambid, P. Debayle, Stability constant of the calcium-citrate (3-) ion pair complex, J. Chem. Eng. Data 36 (1) (1991) 52–54.
[54] J. Schijf, R.H. Byrne, Speciation of yttrium and the rare earth elements in seawater: review of a 20-year analytical journey, Chem. Geol. 584 (2021) 120479.
[55] R.W. Ramette, G. Fan, Copper (II) chloride complex equilibrium constants, Inorg. Chem. 22 (22) (1983) 3323–3326.
[56] J.R. Haas, E.L. Shock, D.C. Sassani, Rare earth elements in hydrothermal systems: estimates of standard partial molal thermodynamic properties of aqueous complexes of the rare earth elements at high pressures and temperatures, Geochim. Cosmochim. Acta 59 (21) (1995) 4329–4350.
[57] W. Bourcier, H. Barnes, Ore solution chemistry; VII, Stabilities of chloride and bisulfide complexes of zinc to 350 degrees C, Econ. Geol. 82 (7) (1987) 1839–1863.
[58] A.J. Graffeo, J.L. Bear, The formation kinetics of some lanthanide oxalate complexes, J. Inorg. Nucl. Chem. 30 (6) (1968) 1577–1584.
[59] K.J. Cantrell, R.H. Byrne, Rare earth element complexation by carbonate and oxalate ions, Geochim. Cosmochim. Acta 51 (3) (1987) 597–605.
[60] S. Hubert, M. Hussonnois, R. Guillaumont, Mise en evidence de l'effet nephelauxetique dans un complexe citrique des elements de la serie 4f, J. Inorg. Nucl. Chem. 35 (8) (1973) 2923–2944.
[61] A. Ohyoshi, E. Ohyoshi, H. Ono, S. Yamakawa, A study of citrate complexes of several lanthanides, J. Inorg. Nucl. Chem. 34 (6) (1972) 1955–1960.
[62] R.J. Giraud, P.H. Taylor, C.-P. Huang, Combustion operating conditions for municipal Waste-to-Energy facilities in the US, Waste Manag. 132 (2021) 124–132.
[63] A.E. Lewis, Review of metal sulphide precipitation, Hydrometall. 104 (2) (2010) 222–234.
[64] Y. Iwata, H. Imura, N. Suzuki, Coprecipitation equilibrium of lanthanoid (III) ions with calcium oxalate, Anal. Sci. 6 (5) (1990) 753–756.
[65] R.D. Shannon, Revised effective ionic radii and systematic studies of interatomic distances in halides and chalcogenides, Acta Crystallogr. Sect. A: Cryst. Phys., Diffr., Theor. Gen. Crystallogr. 32 (5) (1976) 751–767.
[66] D.R. Lide, CRC handbook of chemistry and physics, CRC press2004.
[67] A. Verma, R. Kore, D.R. Corbin, M.B. Shiflett, Metal recovery using oxalate chemistry: a technical review, Ind. Eng. Chem. Res. 58 (34) (2019) 15381–15393.
[68] R.K. Taggart, J.C. Hower, G.S. Dwyer, H. Hsu-Kim, Trends in the rare earth element content of US-based coal combustion fly ashes, Environ. Sci. Tech. 50 (11) (2016) 5919–5926.
[69] C. Erust, A. Akcil, Z. Bedelova, K. Anarbekov, A. Baikonurova, A. Tuncuk, Recovery of vanadium from spent catalysts of sulfuric acid plant by using inorganic and organic acids: laboratory and semi-pilot tests, Waste Manag. 49 (2016) 455–461.
[70] Z. Wiecka, M. Rzelewska-Piekut, M. Regel-Rosocka, Recovery of platinum group metals from spent automotive converters by leaching with organic and inorganic acids and extraction with quaternary phosphonium salts, Sep. Purif. Technol. 280 (2022) 119933.

[71] E.G. Okonkwo, G. Wheatley, Y. He, The role of organic compounds in the recovery of valuable metals from primary and secondary sources: a mini-review, Resour. Conserv. Recycl. 174 (2021) 105813.
[72] R. Golmohammadzadeh, F. Faraji, F. Rashchi, Recovery of lithium and cobalt from spent lithium ion batteries (LIBs) using organic acids as leaching reagents: a review, Resour. Conserv. Recycl. 136 (2018) 418–435.
[73] R. Banerjee, S. Chakladar, A. Mohanty, S. Chakravarty, S.K. Chattopadhyay, M. Jha, Review on the environment friendly leaching of rare earth elements from the secondary resources using organic acids, Geosystem Engineering 25 (3–4) (2022) 95–115.
[74] M.K. Jha, A. Kumari, R. Panda, J.R. Kumar, K. Yoo, J.Y. Lee, Review on hydrometallurgical recovery of rare earth metals, Hydrometall. 165 (2016) 2–26.
[75] J. Mustafa, A.-H.-M. Aya, A.H. Al-Marzouqi, M.H. El-Naas, Simultaneous treatment of reject brine and capture of carbon dioxide: a comprehensive review, Desalination 483 (2020) 114386.
[76] E.C. La Plante, I. Mehdipour, I. Shortt, K. Yang, D. Simonetti, M. Bauchy, G.N. Sant, Controls on CO2 mineralization using natural and industrial alkaline solids under ambient conditions, ACS Sustain. Chem. Eng. 9 (32) (2021) 10727–10739.
[77] U.S.E.P. Agency, Energy Recovery from the Combustion of Municipal Solid Waste (MSW), in: U.S.E.P. Agency (Ed.) 2023.
[78] E. León-Venegas, L.F. Vilches-Arenas, C. Fernández-Baco, F. Arroyo-Torralvo, Potential for water and metal recovery from acid mine drainage by combining hybrid membrane processes with selective metal precipitation, Resour. Conserv. Recycl. 188 (2023) 106629.
[79] C. Lallemand, J.P. Ambrosi, D. Borschneck, B. Angeletti, P. Chaurand, A. Campos, M. Desmau, T. Fehlauer, M. Auffan, J. Labille, Potential of ligand-promoted dissolution at mild pH for the selective recovery of rare earth elements in bauxite residues, ACS Sustain. Chem. Eng. 10 (21) (2022) 6942–6951.
[80] A. Kumari, N.S. Randhawa, S.K. Sahu, Electrochemical treatment of spent NdFeB magnet in organic acid for recovery of rare earths and other metal values, J. Clean. Prod. 309 (2021) 127393.
[81] H. Geng, F. Wang, C. Yan, Z. Tian, H. Chen, B. Zhou, R. Yuan, J. Yao, Leaching behavior of metals from iron tailings under varying pH and low-molecular-weight organic acids, J. Hazard. Mater. 383 (2020) 121136.
[82] H. Tang, W. Shuai, X. Wang, Y. Liu, Extraction of rare earth elements from a contaminated cropland soil using nitric acid, citric acid, and EDTA, Environ. Technol. 38 (16) (2017) 1980–1986.
[83] B. Ji, Q. Li, W. Zhang, Leaching recovery of rare earth elements from the calcination product of a coal coarse refuse using organic acids, J. Rare Earths 40 (2) (2022) 318–327.